

## **EMBEDDED COHESIVE CRACK MODELS BASED ON REGULARIZED DISCONTINUOUS DISPLACEMENTS**

R. Larsson,

Department of Structural Mechanics, Chalmers University of Technology

K. Runesson,

Division of Solid Mechanics, Chalmers University of Technology

M. Åkesson,

Division of Concrete Structures, Chalmers University of Technology,  
Göteborg, Sweden

### **Abstract**

In the context of capturing crack development modeled on the cohesive crack concept, it appears that the issue of how to represent a displacement discontinuity in the FE-environment is crucial for the development of an efficient and robust solution procedure. In the present paper, the qualitative behavior of two crack band models are investigated with respect to the implementation with embedded approximation, which is considered as an alternative to smeared and other discrete crack representations. The formulation is based on a mixed variational formulation that is extended to include internal discontinuities. The major advantage compared to the inter-element representation is that advanced mesh (re)alignment strategies are totally avoided and unstructured meshes are sufficient. The method is applied to two different fracture models at the analysis of a notched concrete plate.

### **1 INTRODUCTION**

A variety of models have been proposed for describing semi-brittle fracture in concrete in the spirit of the "fictitious crack" concept of Hillerborg et al. (1976). In this context, we distinguish two main philosophies: On one hand,

discrete crack models, based on displacement discontinuities, which are represented as interface relations that are established in a successive fashion as the crack develops. The classical approach is to introduce such interface models along inter–element boundaries. Alternatively, the cohesive crack is embedded in the element, cf. Klisinski et al. (1989) and Dvorkin et al. (1990). On the other hand, smeared crack models are represented as continuum tangent stiffness relations that employ a characteristic element diameter in order to convert the crack opening to equivalent element strains, cf. Rots and de Borst (1987) and Dahlbom and Ottosen (1990). In this way an equivalent continuum softening modulus is obtained.

On the basis of the former strategy, two cohesive crack models were derived, by Larsson and Runesson (1995), from a continuum with regularized strong discontinuities, cf. Larsson et al. (1993). The basic idea behind this development was thus to introduce discontinuities along inter–element boundaries, which are realigned according to the result of bifurcation analysis for each load increment. However, it turns out that the required mesh realignment procedure is cumbersome to implement in practice, whereby an alternative strategy is warranted.

The alternative strategy is the "embedded" localization band, where the displacement interpolation allows for a discontinuity within the finite elements. Such a finite element method can conveniently be derived from a three field variational formulation, which incorporates the weak forms of the local equilibrium equation, the strain–displacement relation and the constitutive relationship between the stress and the strain field, as discussed by e.g. Belytschko et al. (1990), Simo and Rifai (1990) and Simo et al. (1993). By decoupling the stress field from the remaining fields via a projection argument on the element level, the resulting FE–method does, in fact, preserve the conventional displacement topology. The major advantage, as compared to the inter–element representation, is that advanced mesh (re)alignment strategies are totally avoided and unstructured meshes are sufficient.

## 2 COUPLED DAMAGE AND PLASTICITY

Denoting by  $\sigma$  the nominal stress tensor of the considered inelastic material, the constitutive law for  $\sigma$  may be written in rate form

$$\dot{\sigma} = \mathbf{D} : \dot{\epsilon} \quad (1)$$

where  $\mathbf{D}$  is the tangent modulus stiffness tensor, which accounts for elastic plastic response coupled to damage. As to the damage, we introduce the (isotropic) damage variable  $\alpha$  as a measure of distributed failure in the material ( $0 \leq \alpha \leq 1$ , where  $\alpha = 0$  indicates the virgin material, whereas  $\alpha = 1$  indicates that the material has undergone complete deterioration). The relation between the "nominal stress"  $\sigma$  and the "effective stress"  $\hat{\sigma}$  is given in the usual way as

$$\boldsymbol{\sigma} = (1 - \alpha)\hat{\boldsymbol{\sigma}} \quad (2)$$

If the yield criterion is expressed in terms of  $\hat{\boldsymbol{\sigma}}$  and a suitable set of internal hardening variables, it is possible to express  $\mathbf{D}$  (as introduced in (1)) as

$$\mathbf{D} = \begin{cases} (1 - \alpha)\mathbf{D}^e - \frac{1}{h}\mathbf{D}^e : \mathbf{g} \mathbf{f} : \mathbf{D}^e & \text{if } \mathbf{f} : \mathbf{D}^e : \dot{\boldsymbol{\varepsilon}} > 0 \text{ (P)} \\ (1 - \alpha)\mathbf{D}^e & \text{if } \mathbf{f} : \mathbf{D}^e : \dot{\boldsymbol{\varepsilon}} < 0 \text{ (E)} \end{cases} \quad (3)$$

where (P) and (E) stand for "plastic" and "elastic" loading, respectively. In (3),  $\mathbf{D}^e$  is the elastic stiffness modulus tensor,  $\mathbf{f}$  is the gradient (in effective stress space) of the yield function  $F$ , whereas  $\mathbf{g}$  is defined as

$$\mathbf{g} = (1 - \alpha)\mathbf{f} + g_A \mathbf{C}^e : \hat{\boldsymbol{\sigma}}, \quad \mathbf{C}^e = (\mathbf{D}^e)^{-1} \quad (4)$$

Here,  $\mathbf{g}$  is the flow direction in accordance with the evolution of damage, whereas  $g_A$  represents the rate of damage development. This is defined via the damage law

$$\dot{\alpha} = 0 \quad (E) \quad (5a)$$

$$\dot{\alpha} = \frac{1}{h} g_A \mathbf{f} : \mathbf{D}^e : \dot{\boldsymbol{\varepsilon}} \quad (P) \quad (5b)$$

Within the proper thermodynamic framework, we may define  $g_A(\hat{\boldsymbol{\sigma}}, A, \alpha) > 0$ , where  $A$  is the "damage force" that "drives" the damage development. Occasionally,  $A$  is denoted the "rate of damage" energy (in analogy with the notion of "rate of fracture energy" in the context of fracture mechanics). It is defined by

$$A = \frac{1}{2} \hat{\boldsymbol{\sigma}} : \mathbf{C}^e : \hat{\boldsymbol{\sigma}} \quad (6)$$

Finally, the (positive) generalized plastic modulus  $h$  is defined as

$$h = \mathbf{f} : \mathbf{D}^e : \mathbf{f} + H \quad (7)$$

where  $H$  is the hardening/softening modulus.

### 3 MIXED VARIATIONAL FORMULATION

Consider a solid, that occupies the domain  $\Omega$  with external boundary  $\Gamma$  as shown in Fig. 1. It is assumed that the displacement field  $\mathbf{u}$  is smooth except that it may be discontinuous across the surface  $\Gamma_s$  with the unit normal  $\mathbf{n}$ . The discontinuity surface divides  $\Omega$  into the sub-domains  $\Omega_-$  and  $\Omega_+$  in such a way that  $\mathbf{n}$  is pointing from  $\Omega_-$  to  $\Omega_+$ . We now propose the decomposition of  $\mathbf{u}(\mathbf{x})$  into a continuous part  $\mathbf{u}_c(\mathbf{x})$  and another part containing the discontinuity, i.e.

$$\mathbf{u}(\mathbf{x}) = \mathbf{u}_c(\mathbf{x}) + [\mathbf{u}]H_s(\mathbf{x}) \quad (8)$$

where  $[\mathbf{u}]$  is the constant jump of  $\mathbf{u}(\mathbf{x})$  across  $\Gamma_s$  and  $H_s(\mathbf{x})$  is the Heaviside function.

Upon introducing a narrow band zone  $\Omega_b$  ( $b$  = band) along  $\Gamma_s$  with the width  $\delta$ , as shown in Fig. 1, a regularized version of the strain rate, cf. Larsson and Runesson (1995), can now be expressed as

$$\boldsymbol{\varepsilon} = \boldsymbol{\varepsilon}_c + \frac{1}{2\delta}(n[u] + [u]n) \quad \text{if } x \in \Omega_b \quad (9)$$

where  $\boldsymbol{\varepsilon}_c$  is the continuous part defined as

$$\boldsymbol{\varepsilon}_c = \nabla^s \mathbf{u}_c = \frac{1}{2}(\nabla \mathbf{u}_c + \mathbf{u}_c \nabla) \quad (10)$$

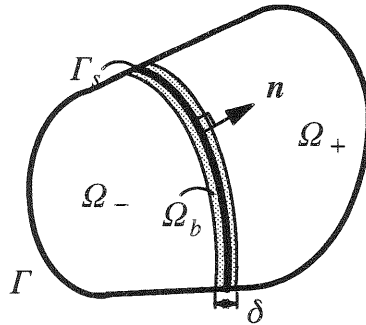


Fig. 1 Solid with regularized singular surface  $\Gamma_s$

In order to invoke the regularized strain into the finite element formulation, it is desirable to construct the discretization such that nodal displacements are continuous across inter-element borders, whereas strains consists of compatible and incompatible (=discontinuous) portions. To this end, we resort to the enhanced strain approach, Simo and Rifai (1990), and propose the three field variational formulation of equilibrium, kinematical and constitutive relations as follows:

$$\int_{\Omega} \boldsymbol{\varepsilon}'_c : \boldsymbol{\tau} d\Omega - W_{ext}(\mathbf{u}') = 0 \quad , \quad \boldsymbol{\varepsilon}'_c = \nabla^s \mathbf{u}' \quad , \quad \forall \mathbf{u}' \in V \quad (11a)$$

$$\int_{\Omega} \boldsymbol{\tau}' : (\nabla^s \mathbf{u}' - \boldsymbol{\varepsilon}) d\Omega = 0 \quad , \quad \forall \boldsymbol{\tau}' \in S \quad (11b)$$

$$\int_{\Omega} \boldsymbol{\varepsilon}' : (-\boldsymbol{\tau} + \boldsymbol{\sigma}(\boldsymbol{\varepsilon})) d\Omega = 0 \quad , \quad \forall \boldsymbol{\varepsilon}' \in E \quad (11c)$$

where the displacements, stresses and strains  $(\mathbf{u}, \boldsymbol{\tau}, \boldsymbol{\varepsilon})$  belongs to the class of functions  $V \times S \times E$ . In the present context,  $(\mathbf{u}, \boldsymbol{\tau}, \boldsymbol{\varepsilon})$  may be considered either as the updated values at the end of each time step, e.g.  $\boldsymbol{\tau} = {}^{n+1}\boldsymbol{\tau}$ , or as the time rate of the state variables, e.g.  $\boldsymbol{\tau} = \dot{\boldsymbol{\tau}}$ . In the former situation,  $\boldsymbol{\sigma} := {}^{n+1}\boldsymbol{\sigma}({}^{n+1}\boldsymbol{\varepsilon})$ , is the stress obtained from integration of the constitutive

relations, whereas in the latter situation  $\sigma := \dot{\sigma}(\dot{\varepsilon})$  is the stress rate that is obtained from the tangent relation (1).

The function spaces  $V$ ,  $S$  and  $E$  are defined as follows:  $V$  is the usual space of compatible (in particular continuous) displacements, whereas  $S$  contains square integrable stresses. As to  $E$ , we are guided by (9) to propose that each strain  $\varepsilon' \in E$  is constructed in terms of a compatible portion and an incompatible portion, defined as

$$\varepsilon' = \varepsilon'_c + \tilde{\varepsilon}' \quad , \quad \varepsilon'_c = \nabla^s u' \quad u' \in V \quad (12)$$

where the enhanced portion  $\tilde{\varepsilon}' \in \tilde{E}$  has the structure

$$\tilde{\varepsilon}' = \begin{cases} \tilde{\varepsilon}'_c + \frac{1}{2\delta}(n\nu' + \nu'n) & x \in \Omega_b \\ \tilde{\varepsilon}'_c & x \in \Omega_c \equiv \Omega \setminus \Omega_b \end{cases} \quad (13)$$

The regular part  $\tilde{\varepsilon}'_c$  is assumed to be square integrable in  $V$ , whereas the vectors  $\nu'$  are square integrable along  $\Gamma_s$ .

From the arguments in Simo and Rifai (1990), the function spaces  $S$  and  $\tilde{E}$  are chosen orthogonal in  $L_2(\Omega)$ . Hence, the stress field  $\tau \in S$  can be eliminated between (11 ac), cf. Larsson and Runesson (1995), whereby (11) may be rephrased as

$$\int_{\Omega} \varepsilon'_c : \sigma(\varepsilon) d\Omega - W_{ext}(u') = 0 \quad (14a)$$

$$\int_{\Omega} \tilde{\varepsilon}'_c : \sigma(\varepsilon) d\Omega + \int_{\Gamma_s} \nu' \cdot (n \cdot \sigma(\varepsilon)) d\Gamma = 0 \quad (14b)$$

## 4 FINITE ELEMENT FORMULATION

### 4.1 Enhanced CST–element

The region  $\Omega$  is discretized into  $NEL$  finite elements  $\Omega_e$ ,  $e = 1, \dots, NEL$ . For a specific element, the displacement and the corresponding compatible strain are interpolated by using the standard compatible shape functions  $N_e$ , which gives

$$u = N_e p_e \quad , \quad \varepsilon_c = \nabla^s u = B_e p_e \quad (15)$$

In this paper, we restrict to piecewise linear approximation, corresponding to the CST–element, for the displacement. Moreover, the stresses  $\tau \in S$  and the enhanced strain  $\tilde{\varepsilon} \in \tilde{E}$  are chosen as piecewise constant (within each  $\Omega_e$ ) such that

$$\tau = \sum_{e=1}^{NEL} \chi_e \tau_e \quad , \quad \tilde{\varepsilon}_c = \sum_{e=1}^{NEL} \chi_e \tilde{\varepsilon}_{ce} \quad , \quad \nu = \sum_{e=1}^{NEL} \chi_e \nu_e \quad (16)$$

where  $\chi_e$  is defined as

$$\chi_e = \begin{cases} 1 & \text{iff } x \in \Omega_e \\ 0 & \text{otherwise} \end{cases} \quad (17)$$

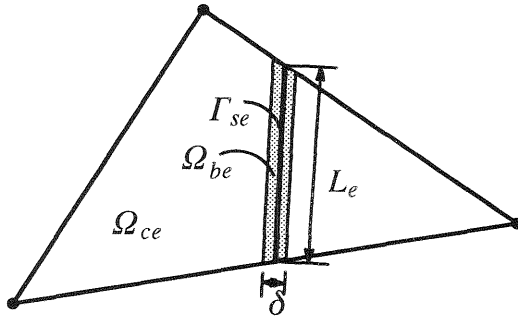


Fig. 2 Constant strain triangle with embedded discontinuity

Since  $S$  and  $\tilde{E}$  are chosen orthogonal in  $L_2(\Omega)$ , we obtain the "orthogonality" (or design) conditions that must be satisfied for each element  $e = 1, \dots, NEL$

$$\tilde{\epsilon}'_{ce} = -\frac{1}{2l_{se}}(n\mathbf{v}'_e + \mathbf{v}'_e n), \quad l_{se} = \frac{A_e}{L_{se}}, \quad A_e = m(\Omega_e), \quad L_e = m(\Gamma_{se}) \quad (18)$$

Upon inserting this expression into (14b), while observing that  $\sigma$  takes the constant values  $\sigma_c$  and  $\sigma_b$  in  $\Omega_{ce}$  and in  $\Omega_{be}$ , as indicated in Fig. 2, respectively, we obtain the simple relationship

$$-\frac{A_e}{l_{se}}\left(1 - \frac{\delta}{l_{se}}\right)(q_c - q_b) = 0 \quad \Rightarrow \quad q_c = q_b \quad (19)$$

where  $q = \sigma \cdot n$ . Hence, the traction is ensured to be continuous across the localization zone. In fact, the traction is continuous across any surface in  $\Omega_e$  with the normal  $n$ .

#### 4.2 Finite Element Equations

Upon invoking the result in (18) into (12) and (13), we may express any strain  $\epsilon'_e \in E(\Omega_e)$  as

$$\epsilon'_e = \begin{cases} \epsilon'_{be} \equiv B_e p'_e + \left(\frac{1}{\delta} - \frac{1}{l_{se}}\right) C_e v'_e & x \in \Omega_{be} \\ \epsilon'_{ce} \equiv B_e p'_e - \frac{1}{l_{se}} C_e v'_e & x \in \Omega_{ce} \equiv \Omega \setminus \Omega_{be} \end{cases} \quad (20)$$

where  $C_e v'_e$  is the matrix representation of the tensor  $(n\mathbf{v}'_e + \mathbf{v}'_e n)/2$  if only shear strains are introduced instead of their tensor counterparts.

Next, by inserting the preceding discretizations into (14ab), we arrive at the discretized formulation

$$\mathbf{A}_{e=1}^{NEL} \mathbf{g}_e(\mathbf{p}_e, \mathbf{v}_e) = \mathbf{A}_{e=1}^{NEL} \left[ \mathbf{b}_e(\mathbf{p}_e, \mathbf{v}_e) - \mathbf{f}_e^{ext} \right] = \mathbf{0} \quad (21a)$$

$$\mathbf{r}_e(\mathbf{p}_e, \mathbf{v}_e) = \mathbf{0} \quad e = 1, 2, \dots, NEL \quad (21b)$$

where the internal element forces  $\mathbf{b}_e$  and  $\mathbf{r}_e$  may be linearized to give the coupled system

$$\begin{bmatrix} d\mathbf{b}_e \\ d\mathbf{r}_e \end{bmatrix} = \begin{bmatrix} \mathbf{K}_e & \mathbf{F}_e \\ \mathbf{F}_e^T & \mathbf{H}_e \end{bmatrix} \begin{bmatrix} d\mathbf{p}_e \\ d\mathbf{v}_e \end{bmatrix} \quad (22)$$

In (22), we have introduced the matrices

$$\mathbf{K}_e = A_e \left( 1 - \frac{\delta}{l_{se}} \right) \mathbf{B}_e^T \mathbf{D}_{ac} \mathbf{B}_e + A_e \frac{\delta}{l_{se}} \mathbf{B}_e^T \mathbf{D}_{ab} \mathbf{B}_e \quad (23)$$

$$\mathbf{F}_e = -\frac{A_e}{l_{se}} \left( 1 - \frac{\delta}{l_{se}} \right) \left( \mathbf{B}_e^T \mathbf{D}_{ac} \mathbf{C}_e - \mathbf{B}_e^T \mathbf{D}_{ab} \mathbf{C}_e \right) \quad (24)$$

$$\mathbf{H}_e = \frac{A_e}{l_{se}} \left( 1 - \frac{\delta}{l_{se}} \right) \left[ \frac{1}{l_{se}} \mathbf{Q}_{ac} + \left( \frac{1}{\delta} - \frac{1}{l_{se}} \right) \mathbf{Q}_{ab} \right] \quad (25)$$

In (25), we have introduced the algorithmic acoustic matrix  $\mathbf{Q}_a = \mathbf{C}_e^T \mathbf{D}_a \mathbf{C}_e$ , which is the matrix equivalent of the tensor  $\mathbf{Q}_a = \mathbf{n} \cdot \mathbf{D}_a \cdot \mathbf{n}$ .

### 4.3 Analysis of Tension Bar

The developed theory for the CST–element can be applied directly for the modeling of semi–brittle fracture of a uniaxially loaded tension bar, that is subjected to prescribed end displacement, as shown in Fig. 3. The stress–strain relation is assumed to be bilinear with constant elastic modulus  $E$  and softening modulus  $H$ . The whole bar is analyzed as one single element with linear approximation of  $u$  in terms of the end displacement  $p_e$  at the right end, while the left end is fixed, i.e.  $\varepsilon_c$  is constant along the bar. The corresponding axial force (stress) is  $b_e (= \sigma)$ , and the tangent stiffness relation is obtained formally from (22) as

$$\dot{b}_e = \hat{K}_e \dot{p}_e, \quad \hat{K}_e = K_e - F_e^2 H_e^{-1} \quad (26)$$

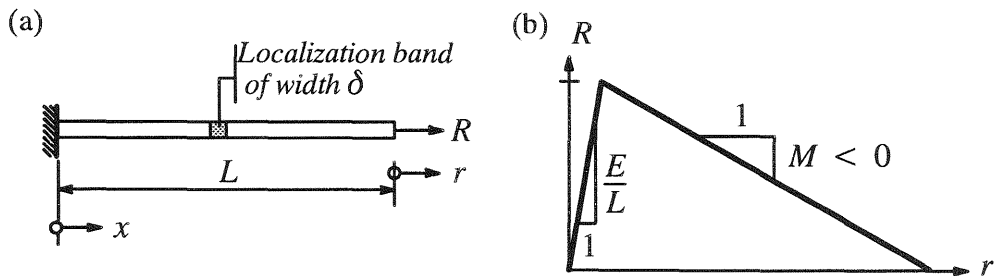


Fig. 3 (a) Tension bar subjected to prescribed end displacement  
(b) Linear structural decay of tensile strength

The pertinent expressions for  $K_e$ ,  $F_e$  and  $H_e$  are given in (23), (24) and (25). Moreover, assuming that elastic loading takes place within the band whereas elastic loading occurs outside together with  $B_e = 1/L$ ,  $C_e = 1$  and  $A_e = l_{se} = L$ , we obtain in quite straightforward manner

$$\hat{K}_e = \frac{E_T}{L} \frac{1}{\frac{\delta}{L} \left(1 - \frac{E_T}{E}\right) + \frac{E_T}{E}}, \quad Q_b = D_b := E_T \quad (27)$$

## 5 CRACK MODELS BASED ON THE RANKINE CRITERION

### 5.1 Rankine Criterion – Preliminaries

Within the constitutive framework outlined above, we shall consider the (tensile) fracture criterion of Rankine for the modeling of semi-brittle fracture in concrete. The criterion is expressed in the "current" principal coordinates as

$$F = \hat{\sigma}_1 - \sigma_t + \hat{K}(\kappa), \quad g_A = \frac{1}{S} \quad (28)$$

where  $\sigma_t$  is the tensile strength,  $\hat{K}$  is an "overstress" which is associated with the hardening variable  $\kappa$ , whereas  $S$  is the material parameter that governs the evolution of damage.

Subsequently, we identify two different special models from the damage–plasticity coupling described above:

The first model is defined by purely plastic response, which is obtained by setting  $S = \infty$ , and assuming  $H$  to be a fictitious material parameter that has to be determined as part of the calibration process.

The second model is defined by choosing the simplest possible damage law and assuming that the virgin material is perfectly plastic, i.e.  $H = 0$ . In this case, it is the damage parameter  $S$  that has to be determined as a part of the model calibration.

### 5.2 Calibration of Crack models

The models are calibrated in mode I, with due consideration to the actual energy release within the crack band. It appears that, for the softening plasticity model, this localization mode is, in fact, the critical one with respect to the critical band orientation at uniaxial stress conditions for incipient fracture. For the damage–plasticity model, a slight rotation from the largest principal stress axis is obtained due to damage development. This rotation is, however, shown to be vanishingly small when the band width tends to zero, as discussed by Larsson and Runesson (1995). Hence, it is sufficient to consider a uniaxial tensile test, where the localization mode is prescribed to mode I.

To this end, let us assume that the bar in Fig. 3 has been subjected to the prescribed displacement  $p_e = r$ , corresponding to the support reaction  $b_e = R$ , such that the peak stress has been reached along the entire length of the bar. For simplicity, it is assumed that the post-peak response is linearly softening with the structural modulus  $M < 0$ , i.e.  $\dot{R} = M\dot{r}$  with  $M = \hat{K}_e$ .

*Softening plasticity model:* For this model, we obtain in uniaxial stress

$$E_T = \frac{H}{E + H} \quad (29)$$

which with  $\hat{K}_e = M$  in (27) yields

$$\frac{H}{\delta} = \frac{\frac{E}{L}M}{\frac{E}{L} - M} \quad (30)$$

We thus obtain the unique element response  $\dot{R} = M\dot{r}$  whenever the ratio  $H/\delta$  satisfies (30). Moreover, the elastic stiffness of the bar is  $E/L$ . For a very short specimen or very large elastic modulus, we then conclude that  $E/L \gg |M|$ . In this case it follows trivially from (30) that we may choose  $H/\delta \approx M$ .

*Damage-plasticity model:* In this case we set  $H = 0$ . This gives

$$E_T = -\frac{\sigma_i}{S} \quad (31)$$

which with  $\hat{K}_e = M$  in (27) yields

$$S\delta = -\sigma_i \left( \frac{1}{M} - \frac{L}{E} \left( 1 - \frac{\delta}{L} \right) \right) \quad (32)$$

It appears, once again, that if  $E/L \gg |M|$ , that the value of  $S$  and  $\delta$  may be obtained from the simple relationship  $S\delta \approx -\sigma_i/M$ .

**Remark:** In the case that the elastic deformation of the test specimen is neglected (or if  $E/L \gg |M|$ ), we obtain the calibration that is pertinent to the fictitious crack concept of Hillerborg et. al. (1976). This means that  $H/\delta$  (or  $S\delta$  for the damage-plasticity model) is calibrated with respect to the released fracture energy  $W_f$  within the crack band, which (due to the assumption about linear softening) gives

$$\frac{H}{\delta} = M = -\frac{1}{2} \frac{\sigma_i^2}{W_f} \quad \text{or} \quad S\delta = -\frac{\sigma_i}{M} = 2 \frac{W_f}{\sigma_i}$$

## 6 NUMERICAL EXAMPLE OF MIXED MODE FRACTURE

Both models have been implemented in the finite element context, where the numerical treatment is based on the fully implicit method. We have analyzed the 50mm thick notched concrete specimen, as shown in Fig. 4, when tension and shear deformations are prescribed simultaneously such that the ratio  $p_t/p_s = 1$  is kept constant throughout the analysis. The present specimen has also been tested experimentally by Nooru-Muhammed (1992) with special attention to mixed mode fracture.

In the experiment, the plate was clamped to the test rig (adhesive plastic glue), whereby displacements are prescribed as shown in Fig. 4. The elastic properties of the (macroscopic) material are taken as  $E = 30GPa$  and Poisson ratio  $\nu = 0.20$ . The tensile yield stress of the virgin material is

$\sigma_t = 3.3 \text{ MPa}$  and the "fictitious crack calibration" was adopted to determine the values of  $H/\delta$  and  $S\delta$  with  $W_f = 100 \text{ J/m}^2$  for the bi-linear decay of the tensile stress in the cohesive zone.

As to the loading, the "plastic zone" constraint, cf. Larsson (1995), was used to control the load increments such that onset of fracture is monitored element-wise in a successive fashion as the loading proceeds. Thereby, the orientation of the internal discontinuities are determined on the basis of the stress state that is present when onset of fracture occurs.

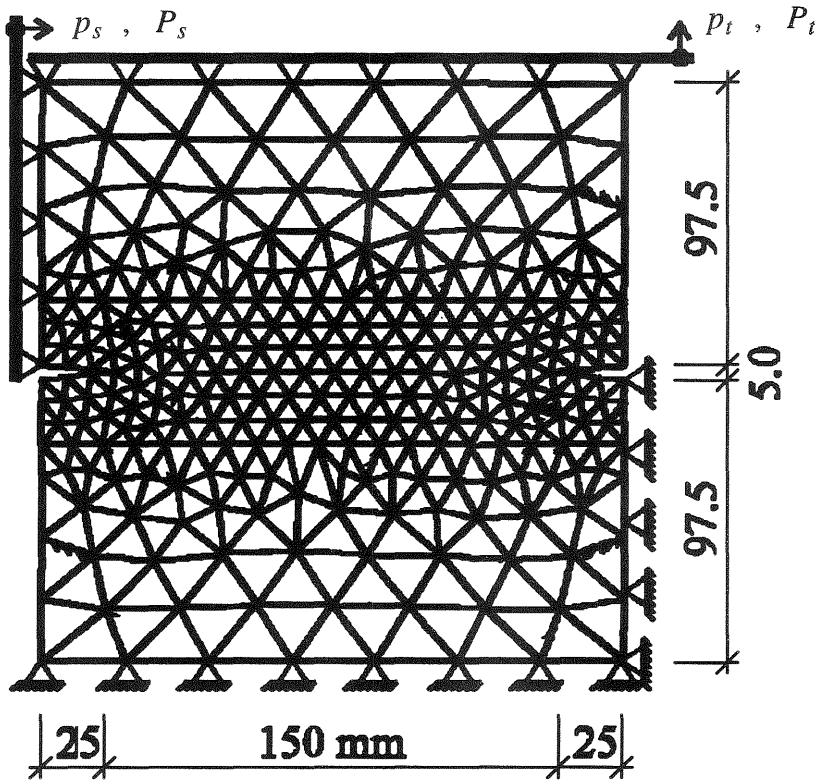


Fig. 4 Geometry, loading and mesh of analyzed concrete plate

The qualitative behavior of the models are compared for a fixed mesh with 508 elements (Fig. 4) when the band width is set to 2mm. The tensile as well as the shear load responses are given in Fig 5ab along with the corresponding experimental results. Note that a quite good agreement is obtained with the experiment. In particular, the damage-plasticity model exhibits a slightly more flexible behavior than does the softening plasticity model; especially, in the right end of the post-peak response. The reason is that the stiffness vanishes for the damage-plasticity model when the material has become completely deteriorated, i.e. when  $\alpha = 1.0$ . As to the tensile response curve, a discrepancy in the pre-peak behavior is obtained due to a different measurement of the "overall" crack opening. Moreover, Figs. 7ab shows the deforma-

tion and crack pattern at the final load-step for the damage-plasticity model, which gives a fairly realistic picture of the global deformation and crack pattern pertinent to the experiment.

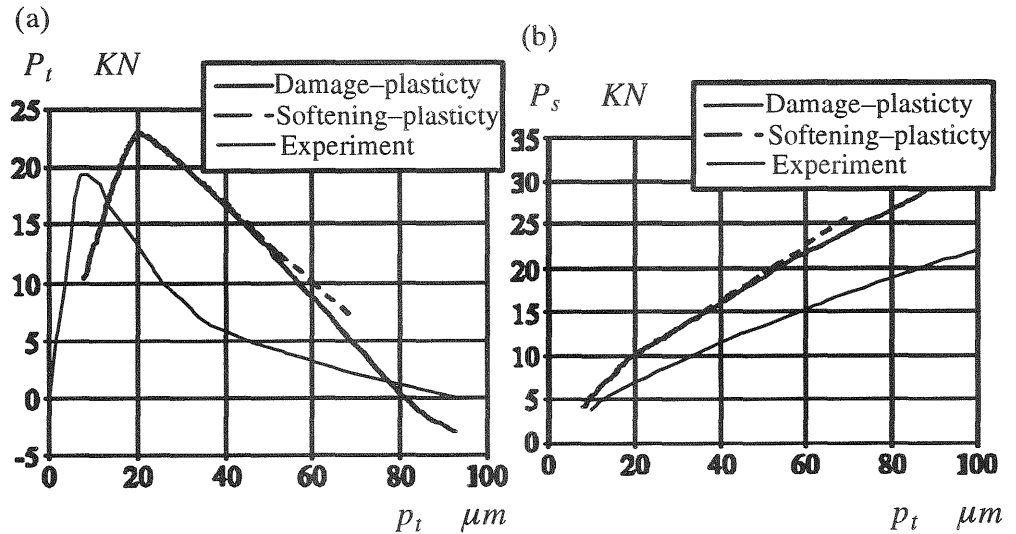


Fig. 5 Tensile and shear response of models as compared to experimental behavior: (a) reactive tensile force versus tensile displacement, (b) reactive shear force versus shear (=tensile) displacement

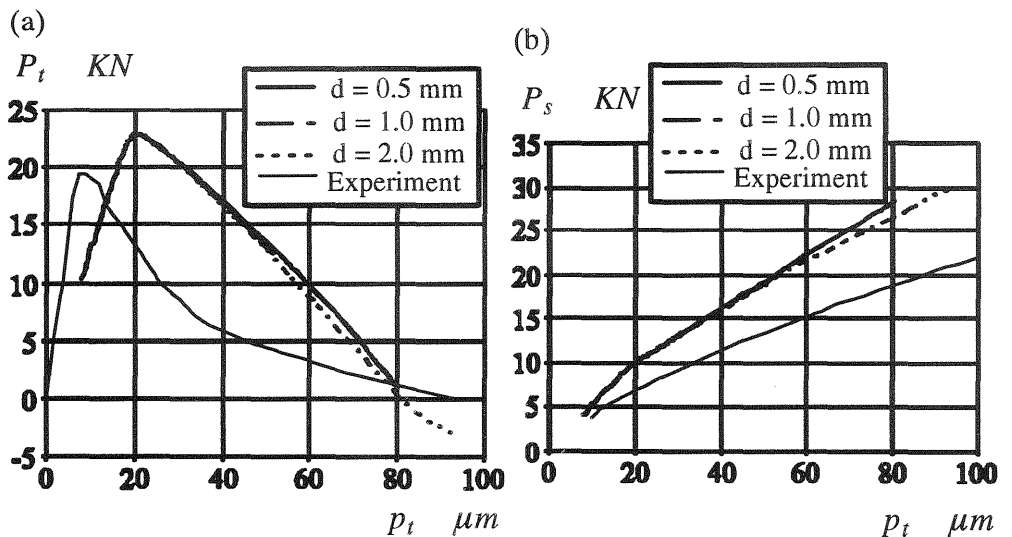


Fig. 6 Model sensitivity to the choice of band width: (a) reactive tensile force versus tensile displacement, (b) reactive shear force versus shear (=tensile) displacement

Finally, we have studied the sensitivity of the models with regard to the choice of band width when the damage-plasticity model is considered. To this end, we consider the choices  $\delta = 0.5mm, 1mm,$  and  $2mm$ . From the cal-

ibration of the model the same model behavior will be obtained in mode I. However, the mixed mode behavior becomes "stiffer" for smaller  $\delta$ , which was also detected for the "inter-element" approach adopted by Larsson and Runesson (1994). This feature of the model is clearly demonstrated in Fig. 6ab, although the general impression is that the response is quite insensitive to the choice of  $\delta$ .

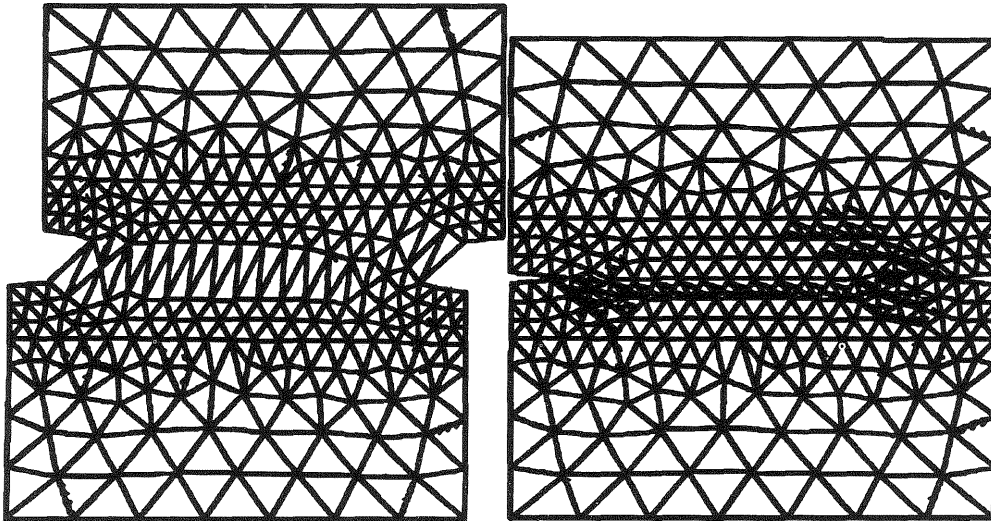


Fig. 7 Global deformation (with exaggerated displacement scale) and crack patterns at final load step for damage plasticity-model

## 7 CONCLUDING REMARKS

On the basis of the developments in Larsson and Runesson (1995), we have in the present paper considered two cohesive crack models in the framework of an embedded localization band. Key ingredients of our analysis are: The concept of discontinuous approximation for capturing localization. The mixed three field variational formulation where a discontinuous strain field was introduced in terms of the element internal variable  $v_e$ .

In this way, both models were implemented for an enhanced CST-element, where, in fact, the classical localization condition is naturally retrieved by the element on the basis of the chosen mixed finite element discretization. We note in particular that, if localization is possible, then the internal discontinuity can be derived explicitly for the rate behavior, in terms of the compatible portion of the strain rate. Moreover, if elastic unloading takes place,  $v_e \equiv \mathbf{0}$  and the element retains the characteristics of the ordinary CST-element.

The models were successfully applied to the analysis of a notched concrete plate. The numerical results obtained from both models shows a fairly good agreement with the experiment.

## 8 REFERENCES

- Belytschko, T., Fish, J., and Englemann, B.E. (1988) A finite element with embedded localization zones. **Comp. Meth. Appl. Mech. Engng.** 70, 59–89.
- Dahlbom, O., and Ottosen, N.S. (1990) Smearred crack analysis using generalized fictitious crack model, **J. Engng. Mech. ASCE** 116, 55–76.
- Dvorkin, E.N., Cuitino, A.M., and Gioia, G. (1990) Finite elements with displacement interpolated embedded localization lines. **Int. J. Num. Meth. Engng.** 30, 541–564.
- Klisinski, M., Runesson, K., and Sture, S. (1991) Finite element with inner softening band. **J. Engng. Mech. ASCE** 117, 575–587.
- Hillerborg, A., and Mod er, M., and Petersson, P.E. (1976) Analysis of crack formation and crack growth in concrete by means of fracture mechanics and finite elements. **Cement and Concr. Res.** 6, 773–782.
- Larsson, R., Runesson, K., Ottosen, N.S. (1993) Discontinuous displacement approximation for capturing plastic localization. **Int. J. Num. Meth. Engng.** 36, 2087–2105.
- Larsson, R. and Runesson, K. (1995) Cohesive crack models for brittle materials derived from localization of damage coupled to plasticity. **Int. J. Fracture** 69, 101–121.
- Larsson, R. (1995) A generalized fictitious crack model based on plastic localization and discontinuous approximation, accepted for publication in **Int. J. Num. Meth. Engng.**
- Larsson, R. and Runesson, K. (1995) Element–embedded localization band based on regularized strong discontinuity, submitted to **J. Engng. Mech., ASCE.**
- Nooru–Mohamed, M.B. (1992) **Mixed Mode Fracture of Concrete: An Experimental Approach**, Ph. D. dissertation, Delft University of Technology.
- Rots, J. G., and de Borst, R. (1987) Analysis of mixed–mode fracture in concrete. **J. Engng. Mech. ASCE** 113, 1739–1758.
- Simo, J.C., and Rifai, M.S. (1990) A class of mixed assumed strain methods and the method of incompatible modes. **Int. J. Num. Meth. Engng.** 29, 1595–1638.
- Simo, J.C., Olivier, J., and Armero, F. (1993) An analysis of strong discontinuities induced by strain–softening in rate–independent solids. **Computational Mechanics** 12, 277–296.

